SIMCor

In-Silico testing and validation of Cardiovascular IMplantable devices

Call: H2020-SC1-DTH-2018-2020 (Digital transformation in Health and Care)

Topic: SC1-DTH-06-2020 (*Accelerating the uptake of computer simulations for testing medicines and medical devices*)

Grant agreement No: 101017578

Deliverable 8.6

Report on 3D finite element simulations

Due date of delivery: 31 December 2022

Actual submission date: 22 December 2022

Start of the project: 1 January 2021

End date: 31 December 2023

This project has received funding from the European Union's Horizon 2020 research and innovation programmeunder grant agreement N° 101017578

Reference

Name	SIMCor_D8.6_Report on 3D finite element simulations_PHI_22-12-2022
Lead beneficiary	Philips Research (PHI)
Author(s)	Michelle Spanjaards (PHI), Valentina Lavezzo (PHI)
Dissemination level	Public
Type	Report
Official delivery date	31 December 2022
Date of validation by the WP Leader	19 December 2022
Date of validation by the Coordinator	19 December 2022
Signature of the Coordinator	

Version log

Issue date	Version	Involved	Comments
08/12/2022	1.0	Michelle Spanjaards (PHI)	First draft by PHI
15/12/2022	2.0	Malte Rolf-Pissarczyk (TUG)	Internal review by TUG
19/12/2022	3.0	Jan Brüning (CHA)	Project Coordinator's review
21/12/2022	4.0	Anna Rizzo (LYN)	Final review and formal checking by LYN
22/12/2022	Final	Jan Brüning (CHA)	Submission by PC

Executive summary

The aim of SIMCor is to establish *in-silico* methods for testing and validation of cardiovascular implantable devices, such as *transcatheter aortic valve implantation* (TAVI) prostheses as well as *pulmonary artery pressure sensors* (PAPS) and make those methods publicly available. *In-silico* simulations can be used to evaluate the safety, efficacy and applicability of medical devices and thus improve the quality of medical devices launched on the market. For this purpose, a numerical model has been developed in WP8 to perform device implantation and device effect simulations for TAVI. The model contains the patient specific (up until now still synthetic) aortic geometry, the TAVI stent geometry and calcification nodules on the valve leaflets. In an effort to reduce the computation time of the model, the TAVI stent was modelled using beam elements. The validity of this method is tested in a convergence study on a *Representative Volume Element* (RVE) of the CoreValve TAVI. Furthermore, a simple method to estimate the post-operative risk of paravalvular leakage is introduced. Note that the model described in this deliverable is also used to perform effect simulations used in deliverable *D9.2 – Device specific models (BIO, M24)* and *D7.6 – Proof of principle of the complete virtual patient generator (TUE, M24)*.

Table of contents

List of figures

List of tables

Acronyms

Acronym	Full name
FE(M)	Finite element (method)
TAVI	Transcatheter aortic valve implant
Nitinol	Nickel-titanium alloy
PVL	Paravalvular leakage
SIMCor	In silico testing and validation of cardiovascular implantable devices
GC	Guiding cylinder
AV node	Atrio-ventricular node
RVE	Representative volume element
CFD	Computational fluid dynamics

Introduction

The aortic valve is prone to dysfunctions as it has to withstand a high-pressure gradient during diastole[1]. One of the most common aortic valve diseases is aortic valve stenosis, which is defined by the narrowing of the valve opening area caused by stiffening of the leaflets due to calcifications that restrict the valve movement. Aortic valve stenosis is most often treated by implantation of a prosthetic heart valve, which can be performed surgically or via *transcatheter aortic valve implantation* (TAVI). TAVI already surpassed surgical aortic valve replacement in terms of absolute procedures performed, as it offers a treatment option for patients with severe risks of surgical complications.

The TAVI-procedure is a minimally invasive technique in which the prosthetic valve is loaded into a delivery device (catheter) and placed into the aortic root[2]. Once the catheter, loaded with the crimped prosthetic valve, is in the correct position, the prosthetic valve is unfolded inside the native aortic valve, thereby pushing the native leaflets out of the way and restoring the correct flow of blood to the aorta and the systemic arteries. Different types of devices exist on the market, which can be divided into two main categories: (1) self-expandable and (2) balloon expandable. The first one makes use of the shape memory ability of the stent to revert to its initial shape upon being released from the catheter, whereas the balloon expandable ones are more rigid and need a pressurized balloon to push them in their final shape. The device deployment technique subject of this deliverable is a self-expandable method.

Despite the high number of procedures, TAVI is still associated with several specific adverse effects. Complications mainly include *paravalvular leakage* (PVL), where blood can flow past the TAVI back into the left ventricle and permanent pacemaker implantation when the TAVI introduces high stress levels on the *atrio-ventricular* (AV) node and bundle of His, causing conduction abnormalities. In this deliverable, an explicit *finite element* (FE) model to perform device implantation and device effect simulations of TAVI in patient-specific aortic geometries is introduced. The simulations can be used to study the effect of the degree of calcifications, which are known to be a risk factor for proper TAVI function, and determine the best device type, optimal size, and position of the device to minimize the risk of post-operative complications such as PVL. Additionally, we present a simple PVL estimation method that can show whether blood can flow past the TAVI back into the left ventricle and give a rough estimation of the regurgitant flow rate.

[1] F. Auricchio, M. Conti, S. Morganti and A. Reali, "Simulation of transcatheter aortic valve implantation: a patient specific finite element appraoch," *Computer Methods in Biomechanics and Biomedical Engineering,* vol. 17, no. 12, pp. 1347-1357, 2014.
[2] C. Russ, R. Hopf, S. Hirsch, S. Sundermann, V. Falk, G. Szekely and M. Gessat, "Simulation of transcatheter aortic valve implantation under consideration of leaflet calcification," *35th Annual International Conference of the IEEE Engineering in Medicine and Biology Society (EMBC),* vol. 35, pp. 711-714, 2013.

Numerical model

In this report an explicit FE model to simulate TAVI deployment is described. Two synthetic patient geometries are used, representing an average female aorta and an average male aorta, respectively. Synthetic calcification nodules are added to the valve leaflets to model the influence of different degrees of calcifications on the risk of paravalvular leakage. CoreValve TAVI devices of different sizes are deployed inside the synthetic geometries.

Problem statement

The problem described in this deliverable is the deployment of a self-expandable TAVI stent inside a synthetic aortic geometry. The stent, and the skirt surrounding the stent, are crimped into the catheter. Inside the catheter, a guiding cylinder is added to keep the outflow part of the TAVI from coming into contact with itself. The catheter is positioned in between the aortic valve, and the catheter covering the crimped device is removed to deploy the TAVI within the aortic annulus. A schematic representation of the different parts of the model is shown in *Figure 1*. Here, the aortic valve leaflets are indicated in green and the calcifications in red.

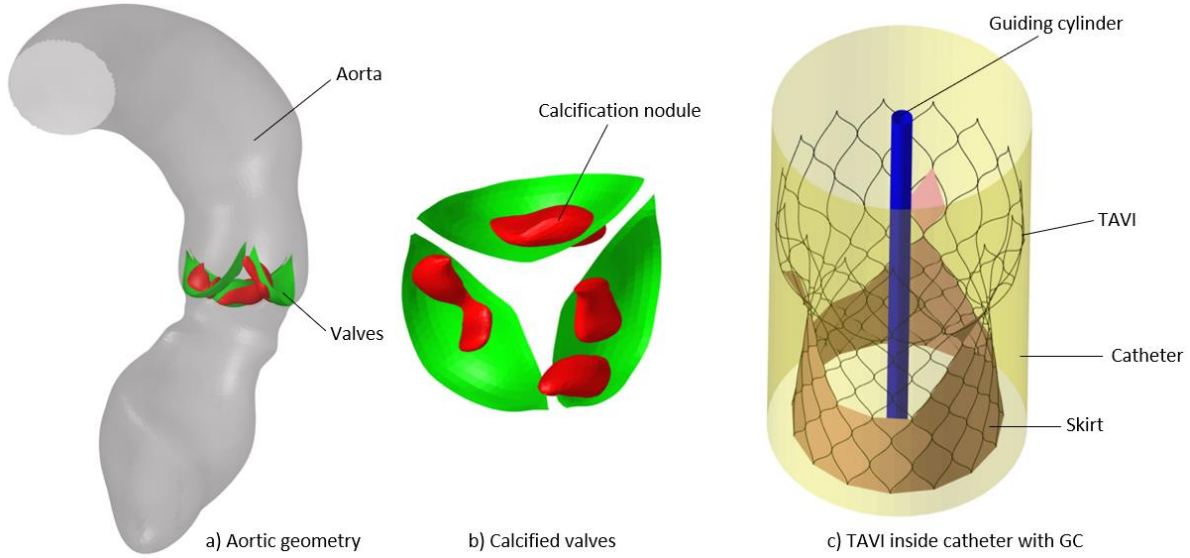

Figure 1: Schematic representation of the used geometry.

Due to licence availability, the HyperMesh software together with the RADIOSS solver is used. It calculates the displacement of each component (i.e., stent, aorta, and leaflets) based on the applied forces and boundary conditions. A similar model is developed in Abaqus, in which the Nickel-Titanium Alloy (Nitinol) material model for the TAVI is already implemented. The explicit integration scheme is mathematically derived from the equation of motion and leads to the following system for each component:

$$\frac{\boldsymbol{M}}{\Delta t^2}\boldsymbol{u}_{n+1} = \boldsymbol{u}_n\left(\frac{2\boldsymbol{M}}{\Delta t^2} - \frac{\boldsymbol{C}}{\Delta t}\right) + \boldsymbol{u}_{n-1}\left(-\frac{\boldsymbol{M}}{\Delta t^2} + \frac{\boldsymbol{C}}{\Delta t}\right) - \boldsymbol{F}_n^{\mathrm{int}} + \boldsymbol{F}_n^{\mathrm{cont}} \qquad (1)$$

where, $\boldsymbol{u}_{n+1}$ is the new unknown displacement, $\boldsymbol{u}_n$ and $\boldsymbol{u}_{n-1}$ represent the displacements of the current and previous time step, respectively and Δt is the time step size. The matrices $\boldsymbol{M}$ and $\boldsymbol{C}$ represent the mass and damping of the system. The internal force $\boldsymbol{F}_n^{\mathrm{int}}$ is calculated using the material model used for a specific component and $\boldsymbol{F}_n^{\mathrm{cont}}$ represent the contact forces exerted by the other components. The true strain ε within each element can now be calculated from the

displacement. Subsequently the Cauchy stress $\boldsymbol{\sigma}$ within each element can be determined using the material model.

Constitutive models

To quantify the risk of paravalvular leakage after TAVI deployment, simplified linear elastic models for the TAVI, the catheter, guiding cylinder and the tissue are first used. The material properties used are listed in *Table 1**Errore. L'origine riferimento non è stata trovata.***. The calcifications are modelled as rigid bodies.

Part	Density [kg/mm^3]	Elastic modulus [MPa]	Poisson ratio
Aorta / leaflets	1 e-9	2	0.4
Skirt	1 e-9	2	0.4
TAVI[3]	6.45 e-9	65000	0.3
Catheter / GC	1 e-9	50000	0.3

Table 1: Material properties of the linear elastic constitutive models used.

Workflow and boundary conditions

The workflow of the numerical model is schematically depicted in *Fugure 2*. First the TAVI is crimped into the catheter (yellow). A guiding cylinder is added (blue) to keep the outflow part of the TAVI from coming into contact with itself. Contacts are defined between the TAVI and the catheter and the TAVI and the guiding cylinder. Next, the catheter and guiding cylinder are removed, and the TAVI is deployed. Additional contacts are now defined between the TAVI and the valve leaflets/calcifications, TAVI and the aorta and the aorta and the valve leaflets/calcifications. Additionally, some boundary conditions are applied in a cylindrical coordinate system where the *z*-axis is specified along the length of the TAVI and the *r*-axis in the radial direction of the TAVI: the nodes on the catheter and the guiding cylinder are restricted from moving in angular direction. During the crimping step, the inflow nodes of the TAVI are restricted to move in *z*-direction and one node on the inflow of the TAVI is restricted to move in angular- and *z*-direction the entire simulation. The top and bottom of the aorta are fixed.

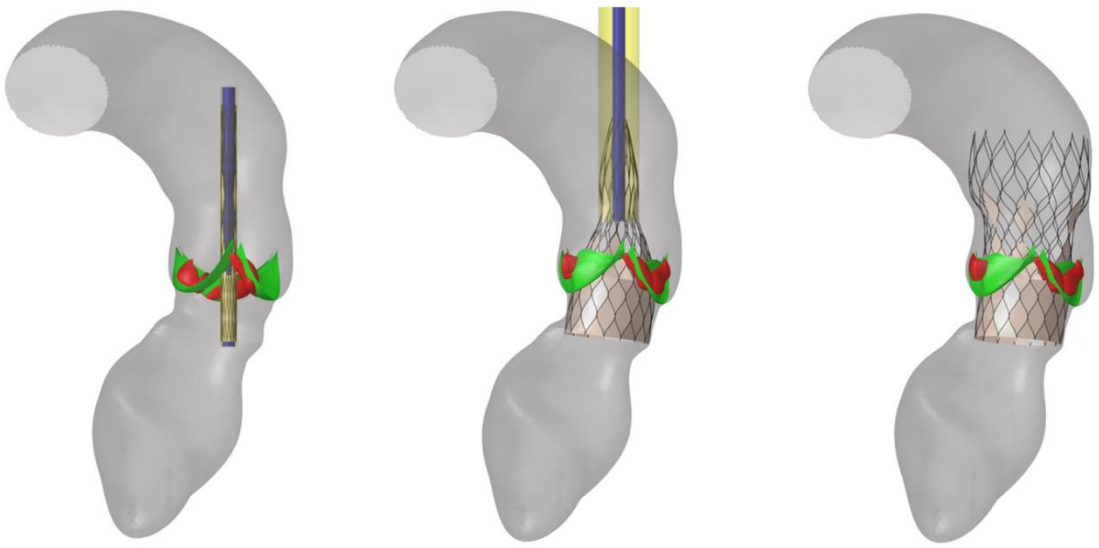

Figure 2: Workflow of the deployment simulations. From left to right: TAVI crimped inside the catheter, TAVI is released from catheter, deployed TAVI inside a synthetic aorta.

[3] J. Oldenburg, F. Borowski and M. Stiehm, "SIMCor Deliverable 8.2: TAVI model," Instititue for ImplantTechnology and Biomaterials, 2021.

Leakage estimation model

The aim of modelling TAVI deployment is to be able to perform a post-operative risk-assessment of PVL for patient specific geometries. In this report we will introduce a simplified model to estimate the risk of PVL without the need of detailed flow simulations. This method could be used as an indicator whether a chosen TAVI is suitable for a specific patient, and thus allow ad hoc assessment for individual cases, as well as larger samples. To this end, the theory of a Poiseuille flow between two parallel plates is used. The circumferential shape of the TAVI and the tissue is obtained at different heights perpendicular to the device's main orientation, within the vicinity of the aortic annulus. This is schematically shown in *Figure 3 (a)*. In the next step, a 3D mesh is constructed filling the area between the TAVI and the tissue. This is schematically shown in *Figure 3 (b)*. After that, this 3D mesh is reduced to a 2D shell mesh positioned in the middle of the gap between the aorta and the TAVI (see *Figure 3 (c)*). Here, the colors indicate the gap size h, where yellow is a large gap and purple is a small gap. For an incompressible Poiseuille flow between parallel plates under the assumption of a small gap the continuity equation reduces to the following equations:

$$\nabla \cdot J = \boldsymbol{u} \nabla \cdot h + h \nabla \cdot \boldsymbol{u} = 0 \qquad (2)$$

where J is the flux, or flow rate, $\boldsymbol{u}$ is the fluid velocity and h is the gap size. For a Poiseuille flow, the velocity between two parallel plates can be calculated as follows[4] [5]:

$$J = -\frac{h^3}{12\mu} \nabla p, \qquad (3)$$

where μ is the fluid viscosity and p the pressure. Under the assumption that the flow rate is purely based on the pressure gradient and a negligible variation in gap size ($\nabla \cdot h$ is assumed to be very small), Equation (2) can be rewritten as follows:

$$-\frac{h^3}{12\mu} \nabla \cdot \nabla p = 0 \qquad (4)$$

A pressure gradient, characteristic to the pressure difference over the valve in the aorta, is prescribed by applying essential boundary conditions on the top and the bottom of the domain. Here, a pressure of 0.13 kPa is prescribed at the top of the domain and a pressure of 0 kPa is prescribed at the bottom of the domain, corresponding to a pressure difference of $\Delta p = 100$ mmHg over the aortic valve. This value corresponds to a characteristic pressure gradient over the valve for healthy adults[6]. Equation (4) is now discretized and solved using the FE method in MATLAB. Using this method, the regurgitant flow rate can be calculated and the gradient of flow can be visualized. Note that this method is only valid under the assumption of small variations in gap size and that the flowlines are purely based on the pressure gradients. As those assumptions are rather strong, we do not aim to quantitatively determine the regurgitant flow but only provide a fast alternative to full *computational fluid dynamics* (CFD) simulations that allows qualitative estimation on whether there is a path along which blood can flow past the TAVI back into the left ventricle, and how effective this path is (is there paravalvular leakage and how severe is this leakage). A more accurate model with less assumptions is work in progress, as is the comparison to the full CFD simulations presented in *WP9*.

[4] T. Papanastasiou, "Lubrication flows," *Chemical Engineering Education,* vol. 23, no. 1, 1989.
[5] A. Christensen and K. Jensen, "Viscous flow in a slit between two elastic plates," *Physical Review Fluids,* vol. 5, p. 044101, 2020.
[6] J. Feher, "Vacular function: Hemodynamics," in *Quantitative human physiology*, Academic Press, 2012, pp. 498-507.

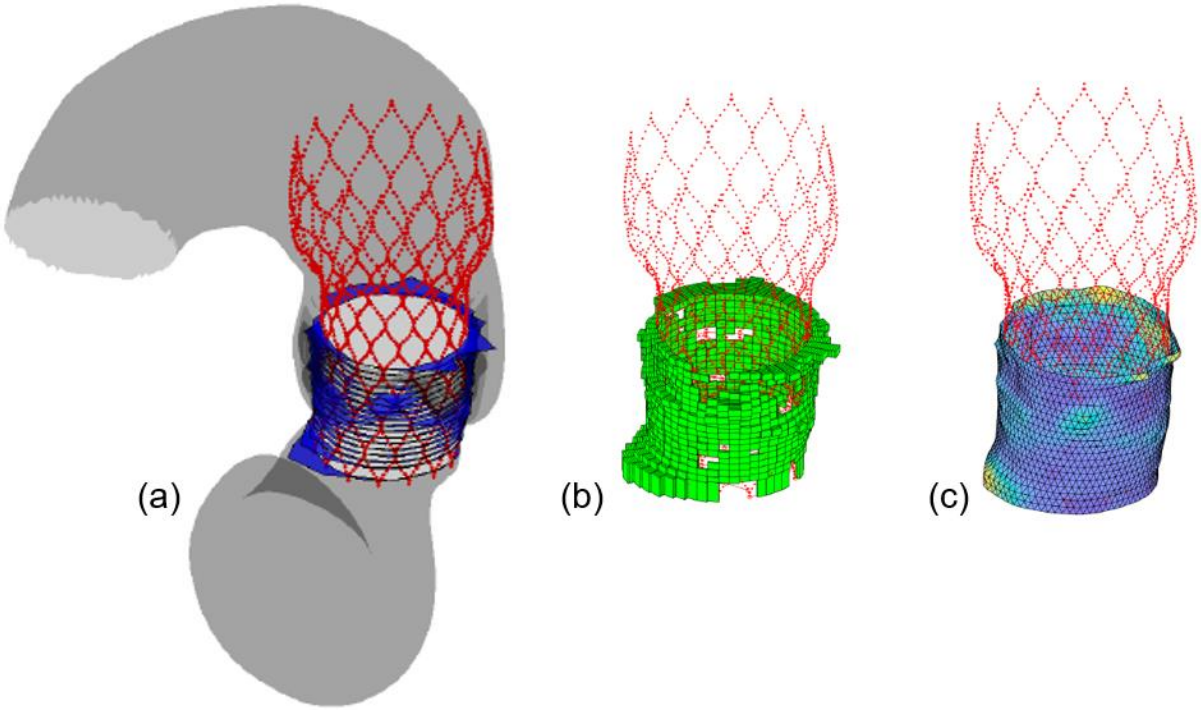

Figure 3: Leakage estimation procedure. Capture circumferential shape of TAVI (white) and aorta (blue) at different heights (a), 3D mesh of the gap between the TAVI and the aorta (b), 2D shell mesh of the gap (c). Colours indicate the gap size (yellow: large gap.

Verification and validation

Verification: convergence study

To verify whether the model is built correctly, convergence tests were performed on a *representative volume element* (RVE), which are reported in this section. One loop of the CoreValve TAVI is chosen as an RVE as schematically depicted in *Figure 4*. An extensional ($\boldsymbol{F}_{\mathrm{t}}$) and compressive ($\boldsymbol{F}_{\mathrm{c}}$) force are applied to the RVE meshed with 3D, linear hexahedral elements as well as 1D beam elements. The RVE and the two applied loads are schematically shown *Figure 5.*

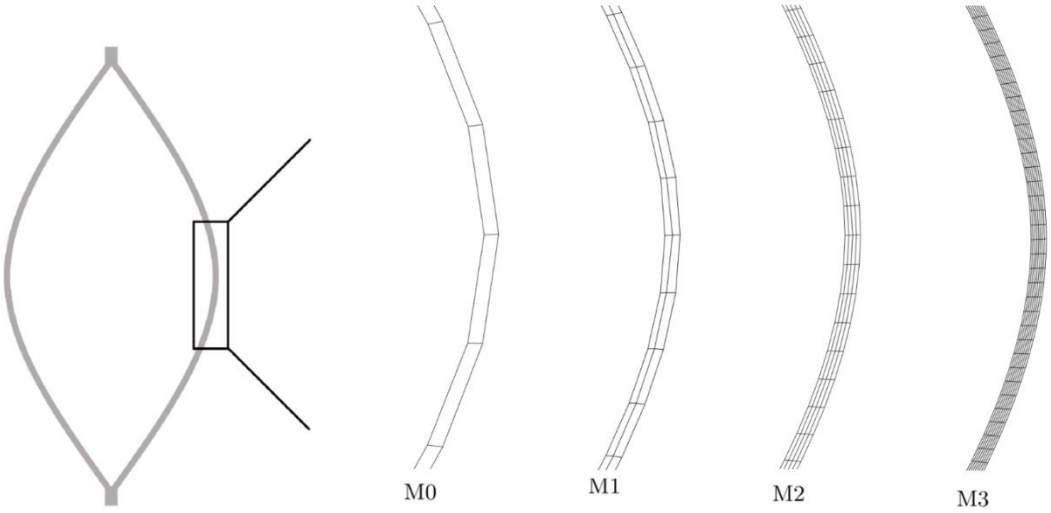

Figure 4: RVE of the CoreValve stent with zoomed in figures of the different 3D meshes used in the convergence study.

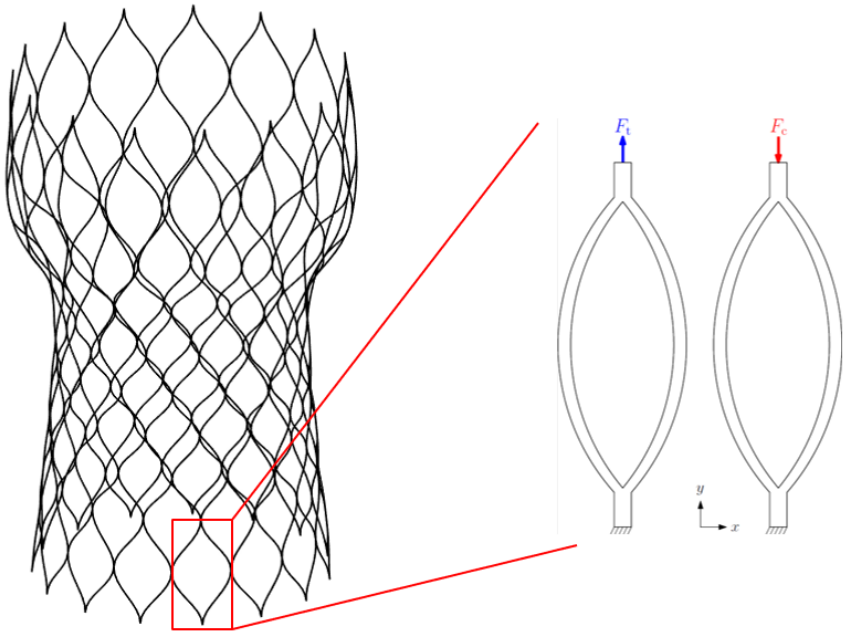

Figure 5: Schematic representation of an RVE of the CoreValve TAVI loaded in extension (left) and compression (right).

The initial mesh M0 consists of 10 elements over the curved length of the RVE and 1 element over the width and thickness of the RVE. The mesh is uniformly refined in all directions. The 3D meshes used in this study are shown in *Figure 4*. More information on these meshes can be found in *Table 2*.

Mesh	N of beam elements	N of 3D elements	N of elements on curved edge	N of 3D elements in cross-section
M0	23	26	10	1x1
M1	44	192	20	2x2
M2	88	1536	40	4x4
M3	176	12288	80	8x8

Table 2: Meshes used in the convergence study on the RVE.

The 3D results in tension and compression are compared to the results using beam elements. First, implicit versus explicit results are compared for mesh M3 in *Figure 6 (a)*, since the two approaches should yield the same result.

This figure shows that an implicit simulation gives approximately the same results as an explicit simulation. Since an explicit formulation is much more robust in non-linear contact problems, such as the problem described in this report, the explicit method is used for the simulations and results for 3D elements are compared to the results using beam elements for the different meshes. *Figure 6 (b)* shows that the results for 3D elements and beam elements converge to the same value upon mesh refinement. For completeness, a 3D simulation is also performed with a full integration element and mesh M2. The results using reduced or full integration are in good agreement and converge to the same value as the results using beam elements upon mesh refinement. *Figure 7* shows the results using integrated beam elements. Again, it can be concluded that the 3D results and the results using beam elements converge to the same value upon mesh refinement.

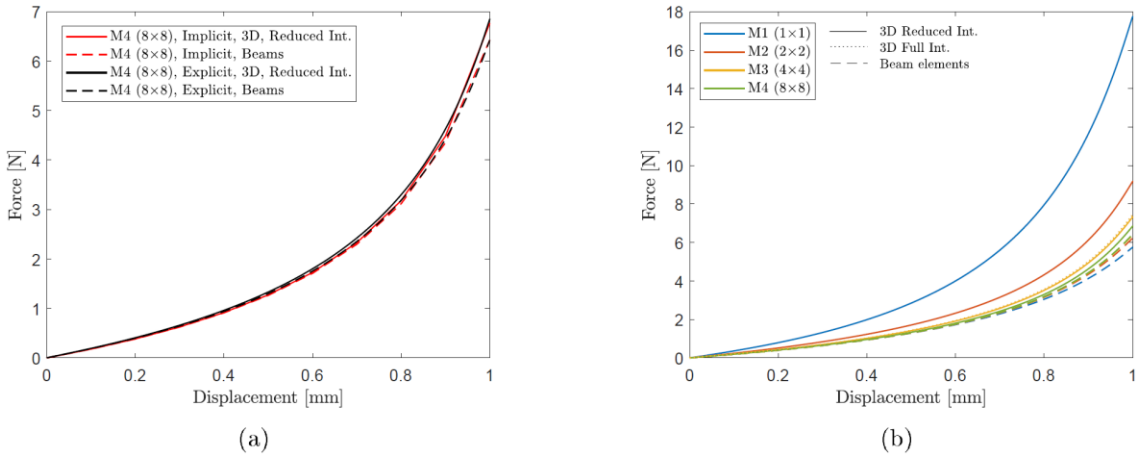

Figure 6: Results of convergence tests under tension. First results of implicit and explicit simulations are compared (a) followed by explicit simulations using 3D elements and beam elements (b).

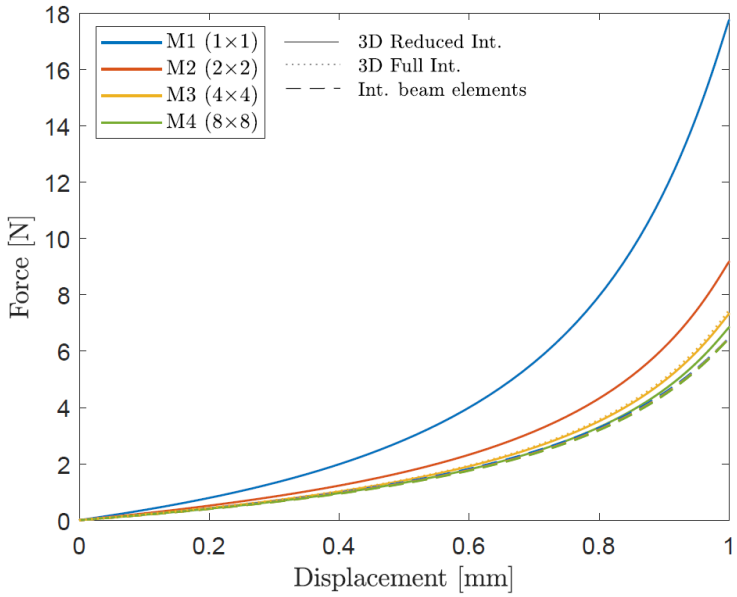

Figure 7: Results of convergence tests under tension comparing 3D elements to beam elements using reduced integration and full integration.

These tests are repeated for a compressive load. *Figure 8 (a)* compares the results of implicit and explicit simulations. This figure shows that an implicit simulation gives approximately the same result as an explicit simulation. In *Figure 8 (b)* the results using 3D elements are compared to the results using beam elements for the different meshes. A simulation using full integration 3D elements is also added for mesh M2. It can be concluded that the results for 3D and beam elements converge to the same value upon mesh refinement.

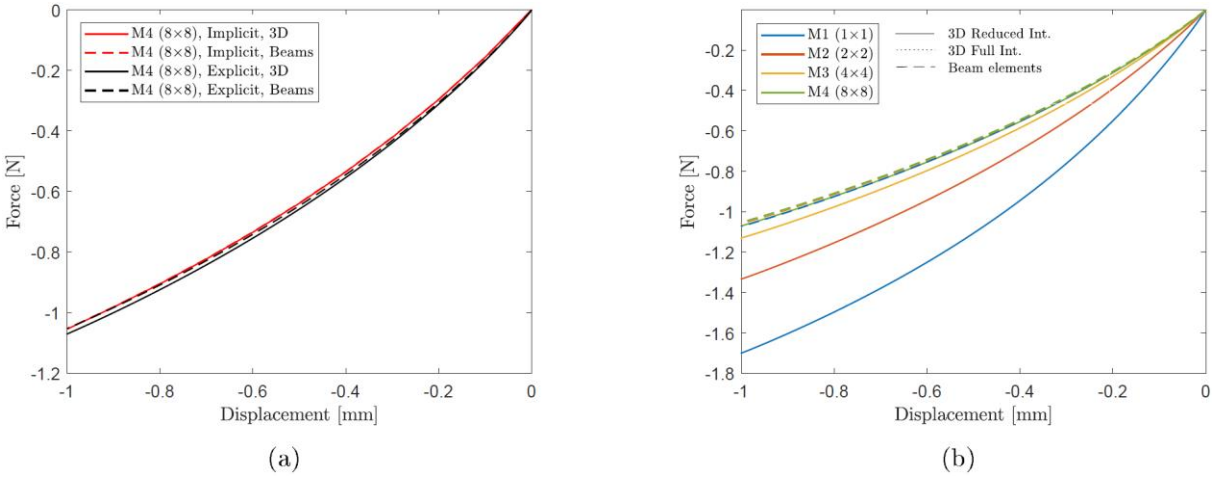

Figure 8: Results of convergence tests under compression. First, results of implicit and explicit simulations are compared (a), followed by explicit simulations using 3D elements and beam elements (b).

The results for 3D elements and beam elements converge to the same value upon mesh refinement for both the tensile and the compressive force. In addition, beam elements are significantly less computationally demanding. Therefore, beam elements are used in the remainder of this report to model the TAVI. The aorta, ventricle, valve, and calcifications are modelled using shell elements.

Validation: crimping test

To validate whether the FE model using beam elements to model the TAVI yields accurate results, TAVI crimping tests are performed using the Abaqus model and results are compared to results from literature[7]. In this paper, the TAVI is modelled using 3D elements, however, to limit computation costs, the mesh of the CoreValve TAVI in this report is constructed out of beam elements. The shape of the TAVI is obtained from a picture in Finotello et al. and therefore, the CoreValve TAVI used in this report is an approximation of the one used in[7]. A radial crimping test is performed on the TAVI using the Nitinol material model with the parameters as described in[7]. The results of a radial crimping test on our beam element mesh and the results obtained from Finotello et al. are plotted in *Figure 9*.

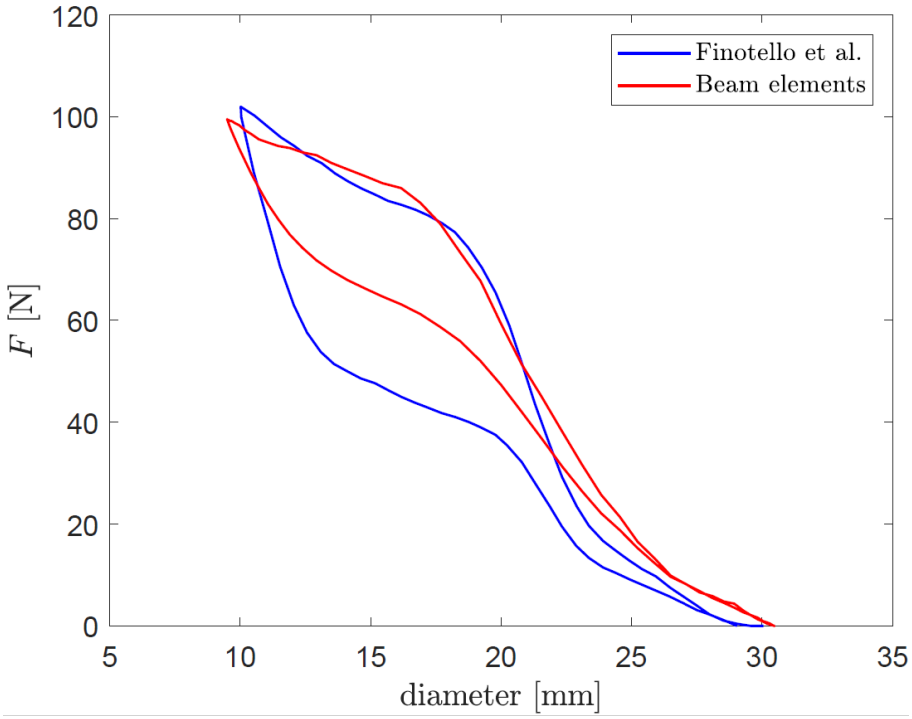

Figure 9: Force-strain diagram of radial crimping test performed on a beam mesh of the TAVI and compared to literature.

From this figure it can be concluded that the force versus strain diagram is captured qualitatively. Since we do not have the exact dimensions of the TAVI struts and the TAVI stent itself, we believe that discrepancies from the experimental curve can be attributed to differences between the real TAVI and our beam element mesh.

[7] A. Finotello, R. Gorla, N. Brambilla, F. Bedogni, F. Auricchio and S. Morganti, "Finite element analysis of transcatheter aortic valve implantation: Insights on the modelling of self-expandable devices," *Journal of the Mechanical Behavior of Biomedical Materials,* vol. 123, p. 104772, 2021.

Results

TAVI deployment

Deployment simulations are performed in synthetic geometries of an average female aorta and an average male aorta. Synthetic calcification nodules are added to study the influence of different degrees of calcified valve. The synthetic geometries are provided by CHA and are available on the VRE. Three different TAVI sizes are deployed inside the synthetic aortas as shown in *Figure 10*.

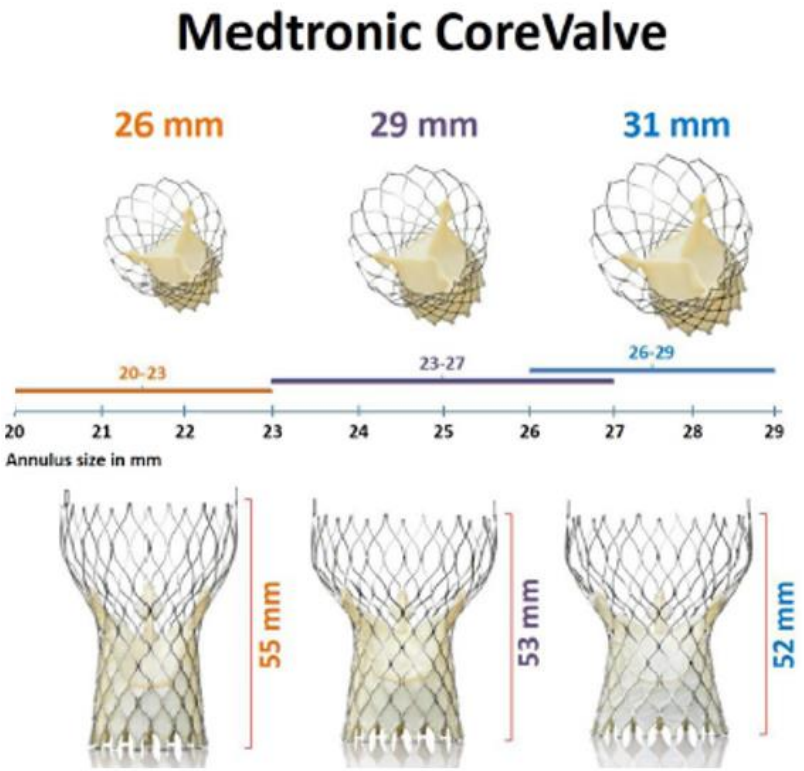

Figure 10: TAVI's of three different sizes indicated by the diameter of the inflow tracks. From left to right: small, medium, large.

In the remainder of this report these TAVI devices will be referenced as small, medium, and large. First, the different TAVI devices are deployed in the average female (annulus diameter = 24.4 mm) and average male (annulus diameter = 27.2 mm) synthetic aorta. Four calcification nodules are placed on the valve leaflets to mimic a medium degree of calcifications. Results of the deployed TAVI inside the female aorta are shown in *Figure 11*. According to *Figure 11* and the annulus size of the female aorta the medium TAVI should be used. *Figure 11* clearly shows that the large TAVI is too large for this aorta and cannot be fully deployed. Therefore, this TAVI will be discarded.

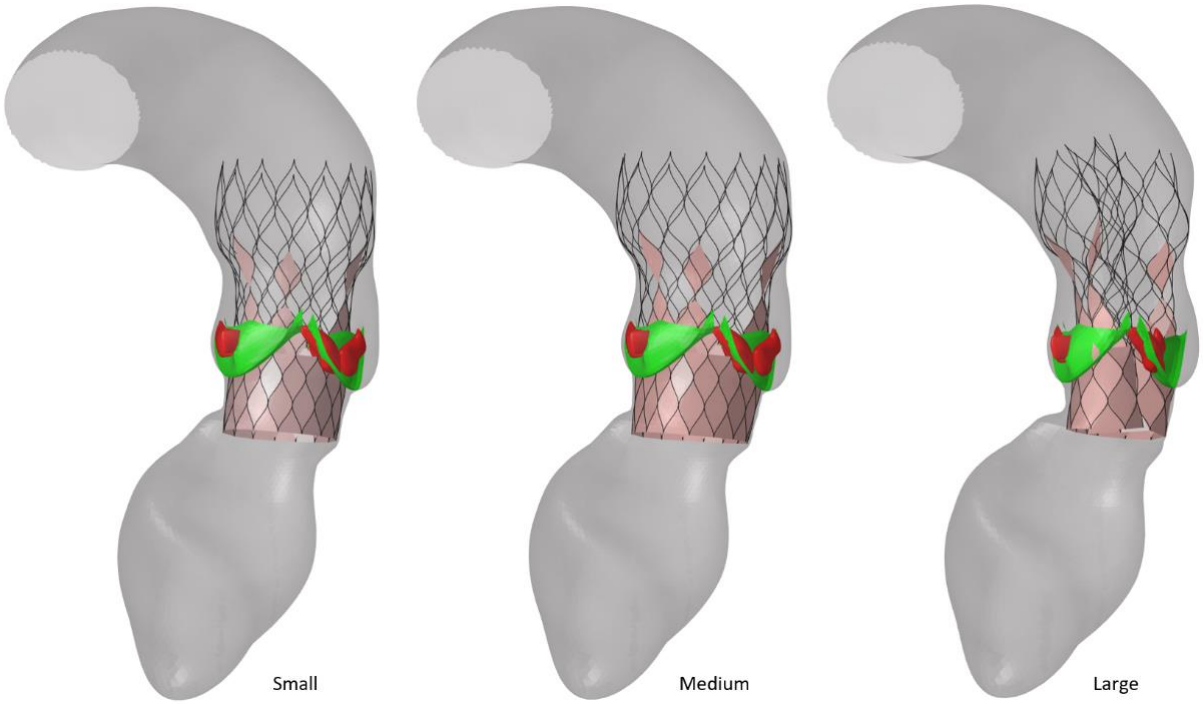

*Figure 11**: Final shape of a deployed TAVI of different sizes inside the synthetic average female aorta.***

Results of the deployed TAVI inside the male aorta are shown in *Figure 12*. According to *Figure 12* and the annulus size of the male aorta, the large TAVI should be the best fit.

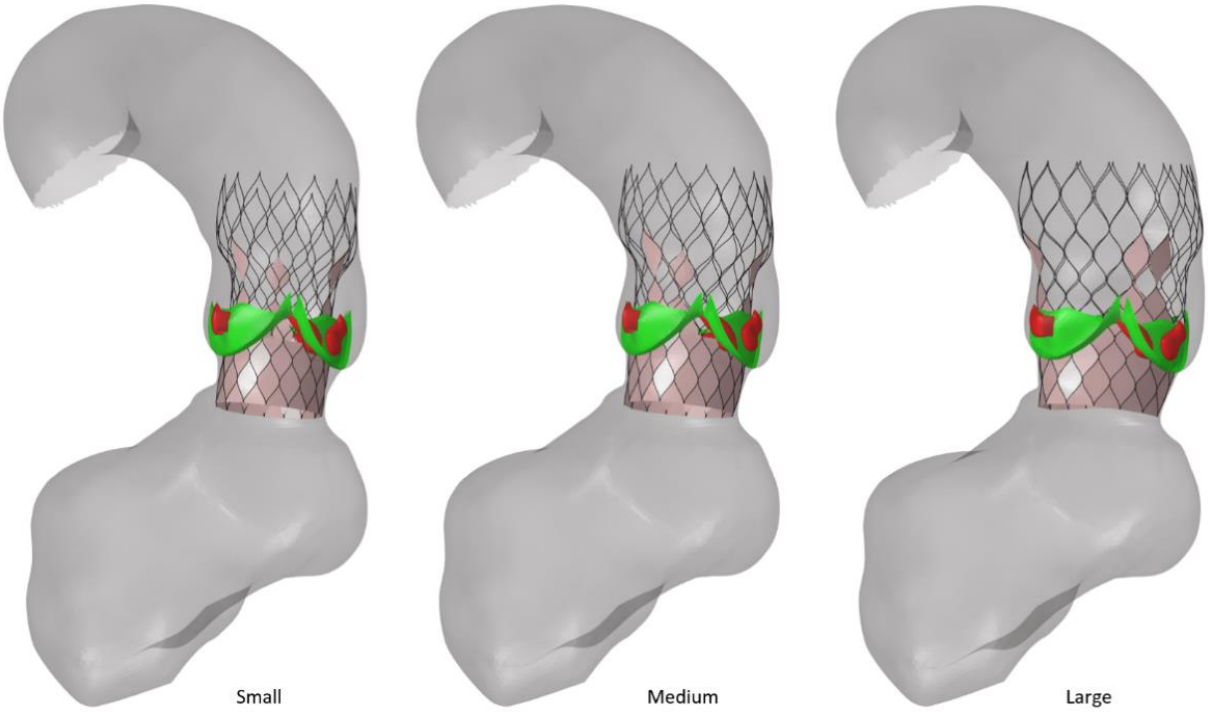

Figure 12: Final shape of a deployed TAVI of different sizes inside the synthetic average male aorta.

Leakage estimation

Next, the leakage estimation model is used to indicate whether blood can flow back past the TAVI into the left ventricle. Results are shown in *Figure 13* for the female aorta and in *Figure 14* for the male aorta.

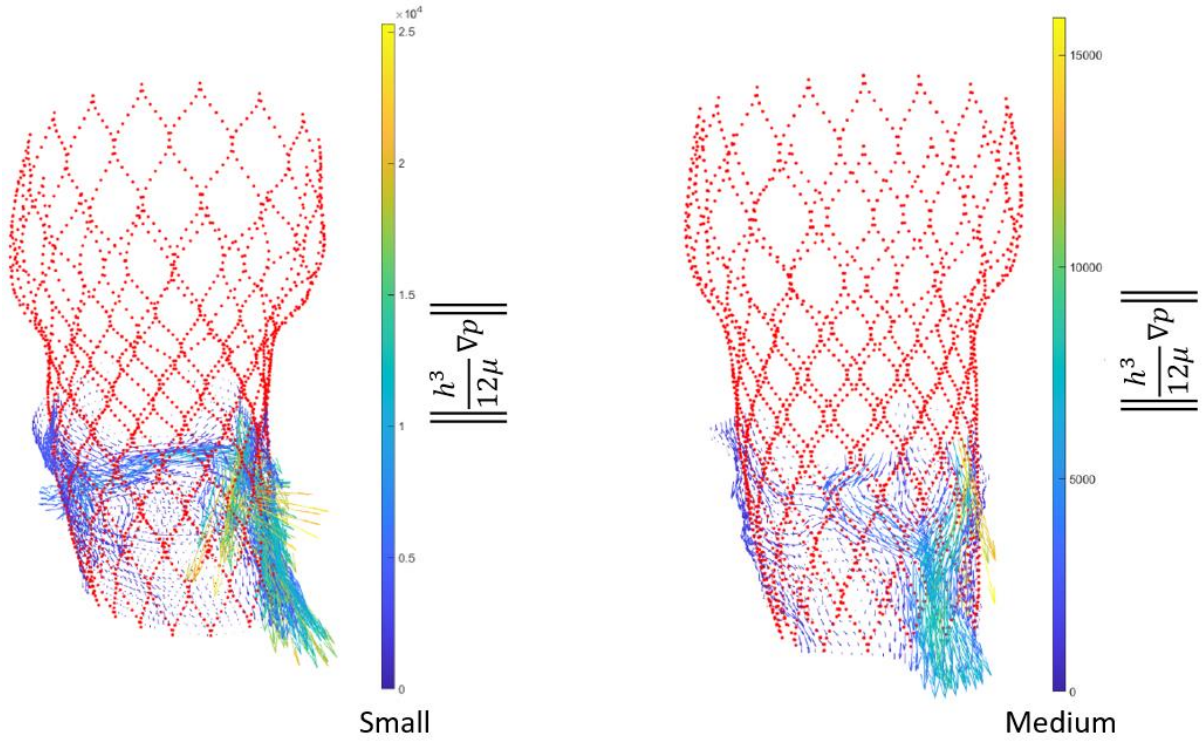

Figure 13: Leakage estimation for the small and medium TAVI deployed in the average female aorta.

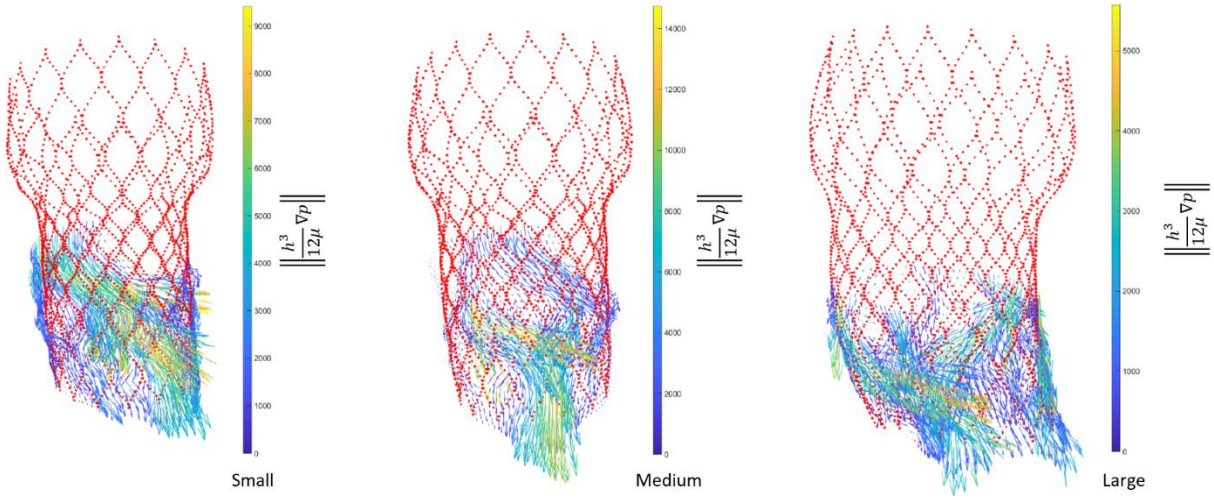

Figure 14: Leakage estimation for the three different TAVI sizes in the average male aorta.

The calculated flow rates for the different TAVI devices are summarized in *Table 3*.

Female		Male	
TAVI size	**Flow rate [ml/s]**	**TAVI size**	**Flow rate [ml/s]**
Small	132.1	Small	103.7
Medium	64.9	Medium	93.6
		Large	58.1

Table 3. Estimated flow rate of fluid flowing past the TAVI in the left ventricle.

From these results it can be concluded that, as expected, a larger TAVI leads to less leakage. However, a larger TAVI might lead to larger AV node compression, especially when calcification nodules are present. This is also undesirable. *Figure 15* shows the P1 major principal stress in the average male aorta for the case of the medium and large TAVI. The results in this figure confirm that higher stresses are induced in the aortic wall when a larger TAVI is deployed.

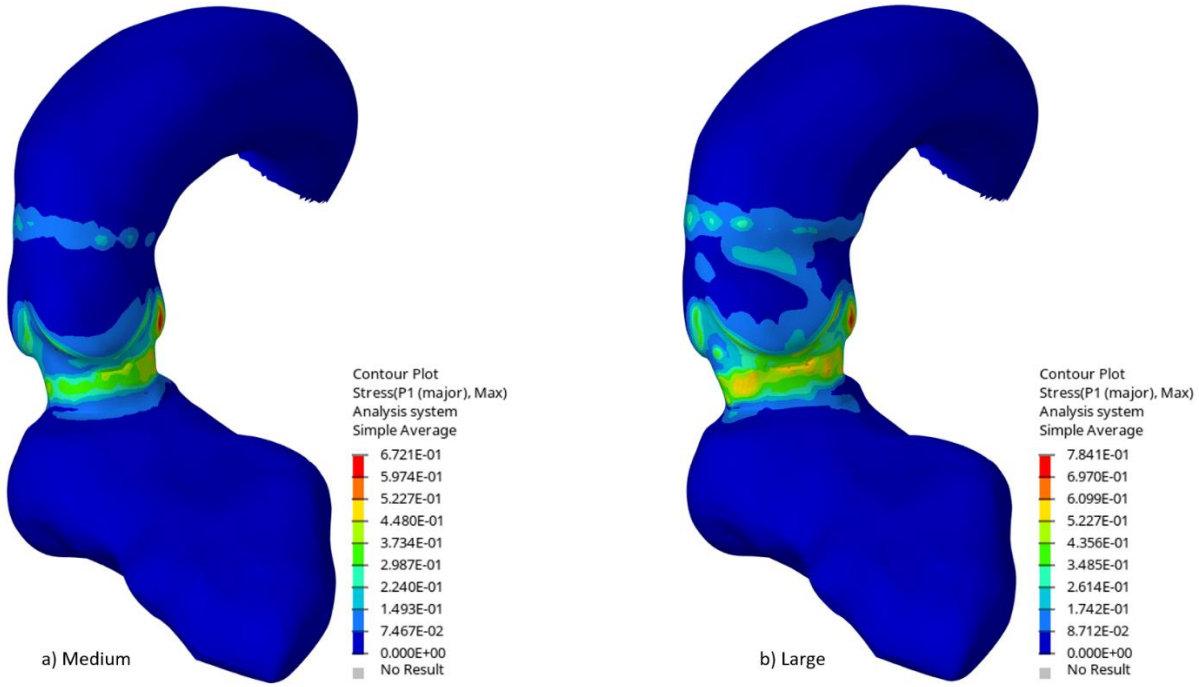

Figure 15: P1 major principal stresses in the aortic wall after deployment of the medium and large TAVI in the average male aorta.

To study the effect of the degree of calcifications on the valve leaflets, simulations are performed for the medium TAVI inside the average female aorta for the case of no calcifications, medium calcified valve, and highly calcified valve. The results are shown in *Figure 16*. Here, the valve with the calcifications is shown in the top (From left to right: no calcifications, medium calcified valve, highly calcified valve).

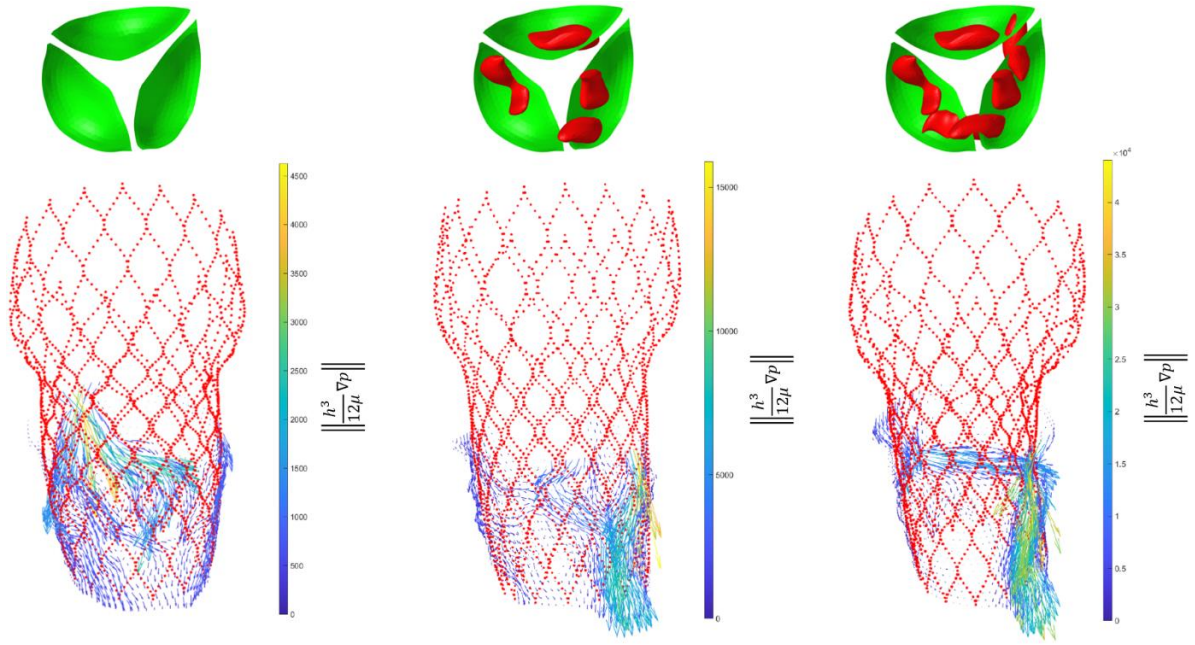

Figure 16: Leakage estimation for the medium sized TAVI deployed in the average female aorta for different degrees of calcifications. On the top the valve leaflets (green) and the calcification nodules (red) are shown.

The simulation results shown previously were performed on the medium calcified valve. For the case of the highly calcified valve, the TAVI is not deployed properly at the bottom. The calcification nodules in this case fuse the valve leaflets together leading to a smaller opening in which the TAVI can be deployed. This in return leads to a more severe case of paravalvular leakage. The calculated flow rates for the different degrees of calcifications is summarized in *Table 4*.

Female (medium TAVI)	
Degree of valve calcification	**Flow rate [ml/s]**
No calcifications	19.9
Medium calcified valve	64.9
Highly calcified valve	185.1

Table 4: Estimated flow rate of fluid flowing back in the left ventricle for different degrees of calcified valve.

Conclusions

We developed a numerical FE model to perform effect simulations of the deployment of a TAVI stent inside a synthetic aortic geometry, including calcified valve leaflets. To speed up the simulation beam elements are used to model the TAVI unlike 3D elements often used in literature. A convergence study is performed on an RVE of the CoreValve TAVI stent to show the validity of this approach. Additionally, we introduced a crude method to estimate the post-operative risk of paravalvular leakage. Note that this method is only valid under the assumption of small variations in gap size. The temporal variations in gap size might be large in reality, and the result will therefore only provide an estimate of PVL. However, the method presented here allows for fast patient-specific profiling of PVL for different aortic pressures.